Strong and ductile platelet-reinforced polymer films inspired by nature: Microstructure and mechanical properties

Lorenz J. Bonderer[a)]
Nonmetallic Materials, Department of Materials, ETH-Zürich, CH-8093 Zürich, Switzerland

André R. Studart
Complex Materials, Department of Materials, ETH-Zürich, CH-8093 Zürich, Switzerland

Jörg Woltersdorf and Eckhard Pippel
Max Planck Institut für Mikrostrukturphysik, D-06120 Halle, Germany

Ludwig J. Gauckler[b)]
Nonmetallic Materials, Department of Materials, ETH-Zürich, CH-8093 Zürich, Switzerland

(Received 6 April 2009; accepted 5 June 2009)

The unique structure and mechanical properties of platelet-reinforced biological materials such as bone and seashells have motivated the development of artificial composites exhibiting new, unusual mechanical behavior. On the basis of designing principles found in these biological structures, we combined high-performance artificial building blocks to fabricate platelet-reinforced polymer matrix composites that exhibit simultaneously high tensile strength and ductility. The mechanical properties are correlated with the underlying microstructure of the composites before and after mechanical loading using transmission electron microscopy. The critical role of the strength of the platelet–polymer interface and its dependence on the platelet surface chemistry and the type of matrix polymer are studied. Thin multilayered films with highly oriented platelets were produced through the bottom-up layer-by-layer assembly of submicrometer-thin alumina platelets and either polyimide or chitosan as polymer matrix. The tensile strength and strain at rupture of the prepared composites exceeded that of nacre, whereas the elastic modulus reached values similar to that of lamellar bones. In contrast to the brittle failure of clay-reinforced composites of similar or higher strength and stiffness, our composites exhibit plastic deformation in the range of 2–90% before failure. In addition to the high reinforcing efficiency and ductility achieved, several toughening mechanisms were identified in fractured composites, namely friction, debonding, and formation of microcracks at the platelet–polymer interface, as well as plastic deformation and void formation within the continuous polymeric phase. The combination of high strength, ductility, and toughness was achieved by selecting platelets that exhibit an aspect ratio high enough to carry significant load but small enough to allow for fracture under the platelet pull-out mode. At high concentrations of platelets, the ductility gets lost because of out-of-plane misalignment of the platelets and incorporation of voids in the microstructure during processing. The designing principles applied in this study can potentially be extended to other types of platelets and polymers to obtain new, hybrid materials with tunable mechanical properties.

I. INTRODUCTION

Ideal materials for structural applications should be simultaneously strong, stiff, and tough. Although in metal alloys this combination can be tailored in a wide range, ceramic and polymeric materials usually lack at least one of these properties. Ceramics are typically strong and stiff but brittle, whereas most polymers are very ductile but are compliant and yield at rather low stresses. One way nature has overcome this problem is by combining platelet-like inorganic building blocks with organic molecules at different length scales to form reasonably strong, stiff, and tough materials such as bone, teeth, and seashells.[1]

The intricate, multiscale structure of platelet-reinforced natural hybrid materials has been extensively studied,[2–6] and substantial progress has been made on understanding their mechanical response.[7–13] However, mimicking the

Address all correspondence to these authors.
[a)]e-mail: lorenz.bonderer@mat.ethz.ch
[b)]e-mail: ludwig.gauckler@mat.ethz.ch
DOI: 10.1557/JMR.2009.0340

structures or the adaption and repair capabilities of nacre and bone using artificial building blocks remains unachieved. Most attempts to mimic the structure of nacre in particular have focused on the reinforcement of polymers with inorganic platelets. However, the volume fractions of the inorganic phase in artificial polymers reinforced with individual platelets is still considerably lower ($\leq$50 vol%) than that in biological structures ($\sim$95 vol%) because of difficulties during dispersion, orientation, and complete infiltration of the platelets with a polymer matrix.[14–18] An alternative approach that circumvents these problems and enables volume fractions of inorganic phase of up to 80 vol% is the infiltration of presintered interconnected lamellar ceramic structures with a polymer[19,20] instead of dispersing individual platelets throughout a polymer matrix. Although a remarkable increase in toughness has been achieved using this approach, the inorganic lamella in these composites are at least one order of magnitude thicker than the inorganic platelets found in biological structures, which can reduce the strength of the inorganic reinforcing lamella.[12]

Besides the challenges during processing, the fact that high-performance platelets are not widely available has also hindered the development and use of hybrid materials with planar reinforcement. Glass flakes, SiC, and AlB_2 platelets of high strength, for example, are hard to produce in large quantities, whereas highly abundant natural platelets such as graphite/graphene, mica, and talcum are difficult to fully exfoliate.[14–18,21,22] When incompletely exfoliated, platelets easily slide against each other, reducing their strength and their ability to reinforce the composites.

The limited industrial applications of platelet-reinforced polymers contrast with the widespread use of fiber-reinforced composites. However, the fact that oriented platelets can carry load in two directions and are thus more efficient than fibers for two-dimensional loading conditions[16] has stimulated further research on the processing of composites with planar reinforcement. Because of its large availability, low price, and small dimensions and thus high strength,[12] most research has concentrated on clay platelets as inorganic reinforcing units in polymers.

Considerable enhancement of strength and stiffness has been achieved at platelet concentrations <10 wt%, especially in the case of clay-reinforced polymers.[18,23] At clay concentrations >10 wt%, the strength of the composites is often lower than predicted by theoretical models.[24] This problem has been associated with difficulties to fully exfoliate and disperse the clay sheets in the polymer matrix, as well as with poor texture and bonding at the organic–inorganic interface.[18,25]

The strengthening effect achieved in clay-reinforced polymers involves (i) the classical load transfer mechanisms that occur in composites with platelets of all sizes,[26] (ii) the cross-linking of the polymer chains between neighboring nanosized platelets,[24,27] and (iii) stiffening caused by ordering/crystallization of the organic matrix in the confined space between the $\sim$1-nm thin clay sheets.[28] The cross-linking effect imparted by clay sheets was recently used to fabricate highly textured clay composites with strength and elastic modulus as high as 400 MPa and 100 GPa, respectively.[28] Because cross-linking reduces the ability of the polymer to deform plastically at high stresses, the resulting composites fractured without any ductility. This contrasts to the combination of high strength and ductility observed in nacre.

In a previous study,[29] we applied some of the structural concepts found in biological materials like nacre to fabricate platelet-reinforced chitosan composites that are simultaneously strong and ductile. High strength and ductility were achieved by using platelets with an aspect ratio that allows for significant strengthening while still taking advantage of the ductile nature of the polymer matrix.

In this paper, we use the same principles to fabricate new platelet-reinforced polyimide films. The mechanical properties of these polyimide-based composites and of the previously reported chitosan-based films[29] are correlated with their underlying structure before and after mechanical loading investigated by transmission electron microscopy. The critical role of the platelet–polymer interfacial bonding on the mechanisms controlling the composite fracture is also thoroughly discussed. Finally, we compare the mechanical behavior of the chitosan and polyimide films reinforced with alumina platelets with that of other planar-reinforced polymers reported in the literature. The structure–property relation derived from this study should aid the design of new artificial hybrid materials combining strength and ductility.

II. MECHANICAL DESIGN OF PLATELET-REINFORCED COMPOSITES

Various models have been proposed to describe the mechanical behavior of platelet-reinforced biological materials.[9–11] To derive general designing principles, we use a simple shear lag model[30] that has been successfully applied to estimate the strength of nacre.[8] The model assumes that the shear forces transferring stress from the matrix to the platelets are constant along the entire platelet, except for a change of sign in the middle of the platelet. This is a reasonable assumption for matrices that yield plastically above a certain threshold stress and for platelets of moderate aspect ratios.

In this model, the yield stress of the composite (σ_y) can be estimated using a modified rule of mixture as follows[30]:

$$\sigma_y = \alpha V_p \sigma_p + \left(1 - V_p\right)\sigma_m \quad , \qquad (1)$$

where V_p is the volume fraction of platelets, σ_p is the platelet tensile strength, σ_m is the yield tensile strength

of the matrix, and α is a factor that depends on the shear strength of the matrix (τ_y), the shear strength of the polymer–platelet interface (τ_i), and the platelet aspect ratio (s).

For aspect ratios higher than a critical value, s_c, the maximal stress on the platelets exceeds their tensile strength, causing platelet fracture and thus a brittle rupture of the composite. In this case ($s > s_c$), α is given by

$$\alpha = 1 - \frac{\sigma_p}{2\tau_{\min} s} \quad , \tag{2}$$

where τ_{min} refers to the lower value among τ_y and τ_i. If $\tau_y > \tau_i$, the interface breaks before the onset of plastic deformation in the polymeric matrix, whereas if $\tau_y < \tau_i$, the matrix yields before the rupture of the platelet–polymer interface.

For aspect ratios lower than s_c, the ductile matrix or the platelet–polymer interface yields before the tensile strength of the platelets is reached, causing pull-out rather than fracture of the platelets within the yielding matrix. Plastic deformation of the polymer leads to a ductile failure of the composite. In this case ($s < s_c$), α is given by

$$\alpha = \frac{\tau_{\min} s}{2\sigma_p} \quad . \tag{3}$$

Composites that fail because of platelet fracture are strong but show no plastic deformation, whereas materials that rupture under the platelet pull-out mode are generally less strong but break in a ductile manner. The critical aspect ratio s_c that defines the type of fracture is given by the following ratio:

$$s_c = \frac{\sigma_p}{\tau_{\min}} \quad . \tag{4}$$

Equation (4) indicates that the critical value s_c and thus the type of the fracture depend directly on the strength of the platelets and the strength of the polymer matrix or of the platelet–polymer interface. The biopolymer matrix and aragonite platelets that constitute nacre, for example, lead to a critical aspect ratio of $\sim$10.[8]

The fact that the structure of nacre has evolved to form aragonite platelets with an aspect ratio ($s \sim 8$) slightly below s_c shows that this biological material has been optimized with respect to both strength and ductility. At an aspect ratio s slightly lower than s_c, ductility is achieved by enabling plastic deformation of the polymeric matrix, whereas high strength is attained by maximizing the aspect ratio of the platelets still under the pull-out mode of fracture.

Inspired by the design principles found in nacre, we selected inorganic platelets and two different polymers that should allow for the fabrication of strong and ductile hybrid materials. Choosing synthetic alumina platelets that are stronger than the aragonite platelets in nacre enables a considerable increase of the aspect ratio s before the critical value s_c is reached [Eq. (4)]. With an estimated σ_p of 2 GPa for the alumina platelets and a τ_{min} of the chitosan or polyimide matrices of maximal 40–50 MPa,[29] the s_c of this material combination is at least 40–50. Under this condition, alumina platelets with an average aspect ratio of $s \sim 40$ carry more load and strengthen the composite more efficiently than the low s platelets in nacre ($s \sim 8$) while still ensuring fracture by the ductile platelet pull-out mode because s is slightly lower than s_c.

The average thickness of 200 nm of the platelets used here is in the same length scale of those in nacre as opposed to the 1-nm-thin clay sheets[18,21,23,24,27,28,31] and the few-micrometers-thick artificial platelets used in other studies.[14,16,26] Alumina platelets with such thickness are presumably thin enough to exhibit high tensile strength[12] but sufficiently thick that, even at high platelet volume fractions, the space between adjacent platelets is large enough not to induce ordering/crystallization that may strengthen but also embrittle the polymer as reported for clay-reinforced polymers.[28] This should enable plastic deformation of the matrix on platelet pull-out combined with conventional load transfer mechanisms between the matrix and the reinforcing platelet.

III. MATERIALS AND METHODS

A. Materials

Alumina platelets were acquired from Advanced Nano Technology Limited (Alusion; St. Welshpool, Australia). Chitosan from crab shells was purchased from Sigma-Aldrich (St. Louis, MO) and used as supplied (practical grade, viscosity > 200 cP for a 1% solution with 1% acetic acid). ^{1}H-nuclear magnetic resonance (NMR) spectroscopy of the chitosan[32] showed a deactylation degree of 80–85%. Polyamic acid obtained from Fujifilm Electronic Materials was used as polyimide precursor (Durimide 115A; Zwijndrecht, Belgium). All other chemicals were analytical grade reagents purchased from Sigma-Aldrich unless otherwise stated.

B. Platelet surface modification

The platelets were surface modified with 3-aminopropyltriethoxysilane (APS) and a functionalized perfluorophenyl-azide (PFPA) as shown in Fig. 1. The functionalized PFPA contained an *N*-hydroxysuccinimide (NHS) active ester group intended to attach to the amino group of APS-functionalized platelets.[33]

APS surface modified platelets were produced by the following route. Ten milliliters of APS was hydrolyzed in 100 mL of a 3:1 (vol:vol) mixture of water and methanol for 1 h. Then, 3.98 g of platelets were added and deagglomerated by ultrasonication for 5 min (80% cycle, 100% amplitude, UP 200s; Dr. Hielscher GmbH, Teltow,

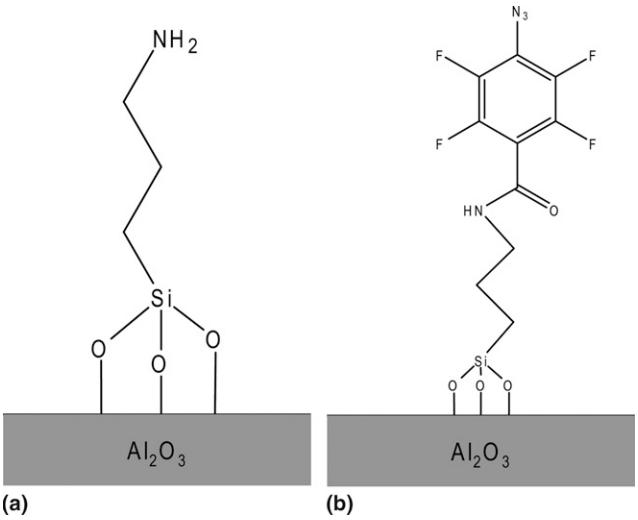

FIG. 1. Supposed surface modification of the alumina platelets with (a) APS and (b) PFPA.

Germany). The suspension was stirred and held at 40 °C for 30 min. Finally, the platelets were washed by repeated centrifugation (Z513K; Hermle Labortechnik, Wehingen, Germany) with pure ethanol.

Further surface modification of the platelet with PFPA was performed by adding 50 μmol PFPA to 1 g of APS-modified platelets in ethanol, followed by stirring for 24 h in the dark. The PFPA-modified platelets obtained were promptly used for the fabrication of composites after washing 8–10 times in a centrifuge. Composites were prepared using either APS or PFPA surface-modified alumina platelets.

C. Surface characterization of the alumina platelets

1. Surface tension

The surface tension of the suspensions was measured using the pendent drop method (PAT1; Sinterface Technologies, Berlin, Germany). After surface modification, the platelets were washed by centrifugation 8–10 times with double-distilled water. Raw (unwashed) and modified platelets were diluted to 1 vol% suspensions, deagglomerated by ultrasonication, and measured.

2. Zeta potential

The zeta potential was measured using an electroacoustic technique (DT1200; Dispersion Technologies, Mount Cisco, NY). Platelet suspensions were prepared as for the surface tension measurements. Additionally, a background ionic strength of 0.01 mol/L KCl was added. The initial pH was set to values <4 using a 1 mol/L HCl solution (Titrisol, Merck, Germany) and gradually increased using a 1 mol/L KOH solution (Titrisol) while acquiring the zeta potential values.

3. Fourier transform infrared spectroscopy (FTIR)

Infrared spectra were obtained with a Perkin Elmer Series 2000 FTIR (Waltham, MA). PFPA surface-modified platelets were washed by centrifugation 8–10 times with ethanol, dried for 12 h at 50 °C, and measured in transmission mode.

4. X-ray photoelectron spectroscopy (XPS)

A monolayer of platelets was dip coated as described in Sec. III. D. Silicon wafers were used as substrates. XPS measurements on the platelet monolayers were performed using a Theta Probe spectrophotometer (Thermo Electron, West Sussex, UK) equipped with a monochromatic Al Kα x-ray source.

D. Fabrication of the composites

The assembly of colloidal platelets at the air–water interface was carried out by slowly dropping an ethanol solution with 1 vol% surface-modified platelets onto a water surface in an 18-mm-diameter cylindrical beaker. Complete coverage of the water surface required ~0.5 and 2 mL of the PFPA- and APS-coated platelet stock solution, respectively. Spreading of the ethanol suspension on the water surface and the slightly hydrophobic nature of the modified alumina surface enabled orientation of the platelets horizontally. The repulsive electrostatic interactions between like-charged platelets at neutral pH allowed for extensive rearrangement of the platelets into a smooth and highly oriented monolayer during sonication. The beaker was typically sonicated for 15–30 min. Platelet layers assembled with this approach were transferred to a 26 × 26-mm^2 glass substrate by manual dipping and were afterward dried in an oven at 50 °C for 30 min.

Chitosan and polyamic acid (polyimide precursor) solutions were used to deposit organic layers on to the platelet layers through spin coating. Chitosan and polyimide were used as polymers because of their high strength, ductility, and good adhesion to alumina. Chitosan was dissolved in aqueous solutions of 2 wt% acetic acid (0.34 mol/L) at concentrations of 0.25 to 3 wt% at least 24 h before use. A commercial 15 wt% stock solution of polyamic acid was diluted with 1-methyl-2-pyrrolidinone (NMP) to change the polymer concentration within a range from 6 to 15 wt%. The thickness of the organic layer and thereby the final volume fraction of alumina platelets was controlled by changing the polymer concentration in the spin-coating solution (Fig. 2).

Spin-coating was conducted on a custom built apparatus by depositing polymer solutions of various concentrations onto a static substrate and subsequently spinning the coated substrate at predetermined speeds. Approximately 1 mL of chitosan solution was spun at 2000 rpm

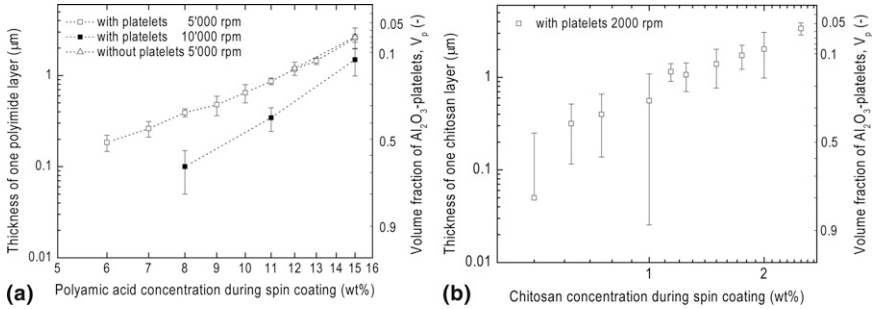

FIG. 2. Thickness of the deposited (a) polyimide and (b) chitosan layer as a function of the polymer concentration in the solution used during spin coating. The volume fraction of platelets shown as the secondary axis was calculated from the measured polymer layer thickness, assuming fully dense layers of 200-nm-thick platelets.

for 40 s and was afterward dried at 50 °C in air. For the polyimide samples, 0.4 mL of polymer solution was spun at 1000 rpm for 15 s, followed by a 15-s rest before spinning the coated substrate again at 5000 or 10,000 rpm for 40 s. The as-deposited wet polyamic acid layers were soft baked on a hot plate at 120 °C for 60 s under nitrogen flow for solvent removal.

Multilayered organic–inorganic films were fabricated by sequential dipping and spin-coating steps. Chitosan matrix composites typically contained 8–10 platelet layers, whereas polyimide composites contained 15 platelet layers. The first and last deposited layers were always made out of polymer. After deposition of all layers, the polyimide matrix composites were dried in vacuum (<0.1 mbar) at 70 °C for 24 h, before curing at 300 °C for 30 min under argon atmosphere to convert the polyamic acid to polyimide. A heating/cooling rate of 200 °C/h was used for curing. Almost complete conversion to polyimide was confirmed by FTIR. After fabrication, the composites were stored at room temperature in a relative humidity of 20–50%.

The volume fraction of platelets, V_p, in the final composite was controlled by changing the concentration of polymer in the solution used during spin-coating. V_p was calculated from the combined average thickness of one organic and one inorganic layer, assuming fully dense inorganic layers of 200 nm thickness.

E. Differential scanning calorimetry

Glass transition temperatures were determined with a Mettler Toledo DSC 822e (Greifensee, Switzerland) differential scanning calorimeter (DSC), calibrated with indium. Polyimide samples of ~2 mg were heated from 25 to 400 °C and cooled down to 25 °C with a heating and cooling rate of 10 °C/min.

F. Mechanical evaluation

The mechanical properties of free-standing hybrid films were measured under tensile mode in a universal mechanical testing machine (Model 5864; Instron, High Wycombe, UK). Test specimens were obtained by peeling off the films from the substrate with a razor blade and cutting the freestanding films into 2- to 3-mm-wide and 20- to 25-mm-long strips. For mechanical testing, the strips were held with custom-made clamps at a distance of 12–18 mm. Because the number of inorganic layers was kept constant, composites with lower organic content and thus higher volume fraction of platelets were thinner and more sensitive. This increased the chance of damaging and breaking the freestanding films during handling before mechanical evaluation. To avoid damage of the composite before mechanical testing, some of the films were coated with a 10-µm-thick polyimide layer that functioned as a protective substrate on one side of the sample. In these cases, the mechanical properties of the composites can be determined by subtracting the previously known force-deformation behavior of the polyimide substrate alone from the overall force-deformation curve obtained for the composite/substrate bilayer.[34] This method enables the mechanical evaluation of thin and highly loaded composites that are too fragile to be tested as completely freestanding films. Comparative tests between free-standing and composite/substrate bilayers with samples containing low platelet volume fractions showed good agreement between the obtained stress-strain curves, validating the use of bilayers for the mechanical evaluation of composites at high platelet volume fractions. Reported data on yield strength, elastic modulus, and strain at rupture are averages of five different stripes of the same sample.

G. X-ray diffraction

The orientation of the platelets in the polymer matrix was measured by x-ray diffraction using a rocking curve (θ scan) technique.[35] This method corrects tilt-induced defocusing and absorption effects with an accurately measured θ-2θ scan. The calculations were performed using the software TexturePlus,[36] which was kindly provided by Mark Vaudin, NIST, Gaithersburg. The full width at half maximum (FWHM) of the corrected rocking curve was used as a measure of the degree of platelet

orientation. The θ and θ-2θ scans of the alumina 0012 peak (2θ = 90.7°) were measured in a Siemens D5000 powder diffractometer (Siemens, München, Germany). Typical acquisition time per scan was 8 h.

H. Transmission electron microscopy: Sample preparation and investigation

Specimens appropriate for transmission electron microscopy (TEM) were prepared using a refined cross-section technique: After fixing the samples between silicon blocks, slides were cut, embedded in epoxy, and divided into small parts containing the areas of interest in the center. After grinding and dimpling, these parts were subsequently glued on specimen holders. The thinning to electron transparency has been performed by ion milling using the precision ion-polishing system PIPS 691 (Gatan, Pleasanton, CA).

The microstructural characterization of the interlayers was performed using a high-resolution/scanning transmission electron microscope (HREM/STEM) Philips CM20 FEG (Amsterdam, The Netherlands), which is equipped with a thermal supported field emission gun (coefficient of spherical aberration of the objective lens, C_s = 2.0 mm; point to point resolution, 0.24 nm) operating at 200 kV. Besides the methods of diffraction contrast and of selected area diffraction, the high-resolution atomic plane imaging technique is applied, which is caused essentially by the phase contrast.

IV. RESULTS AND DISCUSSION

A. Fabrication of the composites

The conditions used during the fabrication of the composites strongly affected their final microstructure, particularly the final volume fraction and the degree of orientation of the platelets in the hybrid films. The platelet volume fraction (V_p) is determined by the concentration of polymer in the solution used during spin coating. Solutions with a high polymer concentration led to thick organic layers and thus low platelet volume fractions as shown in Fig. 2. The spinning speed also influenced the thickness of the deposited polymer layer. Higher speeds result in thinner polymer layers and higher V_p. In general, spin-coated polyimide layers exhibited little deviation in thickness, whereas the thickness of chitosan layers scattered significantly (Fig. 2). The poor control over the thickness of the chitosan films was caused by extensive swelling and partial removal of chitosan during the dip coating step. The higher reproducibility during processing of the polyimide-based films enabled better control over the composite final platelet content. This also allowed for more reliable preparation of polyimide-based composites with high V_p compared with the chitosan matrix films.

Hybrid films containing platelet volume fractions up to 0.5 exhibited a brick-and-mortar structure with strongly oriented platelets surrounded by a polymeric matrix as shown in Fig. 3(a). The platelets are clearly aligned parallel to the composite surface and are relatively homogeneously distributed in the polymer matrix. Platelets became slightly misaligned for increasing inorganic contents, as indicated by the FWHM of the corrected rocking curves shown in Fig. 4. The misalignment is, however, <8° for the majority of platelets in composites with platelet volume fractions up to 0.5. In general, we observed that misalignment increases with the number of platelet layers in the composite. This explains the slightly better orientation in the chitosan matrix composites at low inorganic contents compared with the polyimide-based materials. Polyimide composites contained 15 platelet layers, whereas the chitosan composites contained 8–10 platelet layers.

The enhanced hydrophobicity of the PFPA-modified platelets led to a stronger adsorption of these platelets at the air–water interface during the formation of the Langmuir type film. This effect decreased by about three times the amount of suspension necessary to form a full monolayer in comparison with the APS-modified platelets. The lower amount of suspension needed in the case of PFPA-modified platelets reduced the concentration of nonadsorbed platelets in the water subphase. This decreases the likelihood of transferring more than one monolayer during each dipping step, resulting in more even and aligned platelet layers. The FWHM of composites of similar V_p containing PFPA-modified platelets was ∼1° lower than for composites with APS-modified platelets (Fig. 4).

Large-scale fabrication of platelet-reinforced bulk composites with the layer-by-layer method used here seems unlikely because of the manual dip coating of the platelets from a Langmuir type film. However, the higher degree of platelet orientation, the fewer platelet agglomerates, and the absence of phase separation into platelet-rich and platelet poor phases at a wider range of platelet volume fractions compared with conventional large scale methods such as melt extrusion of clay reinforced polymers[18] makes this laboratory-scale method appropriate for a thorough study of the mechanical behavior of platelet-reinforced composites. Once the concept of mechanical reinforcement by platelet has been shown on laboratory-scale samples, further studies are needed for the development of large-scale fabrication methods with a comparable degree of control over the composite structure.

B. Microstructure and mechanical properties

The mechanical properties of the composites are isotropic in the plane of the platelets and extended strongly

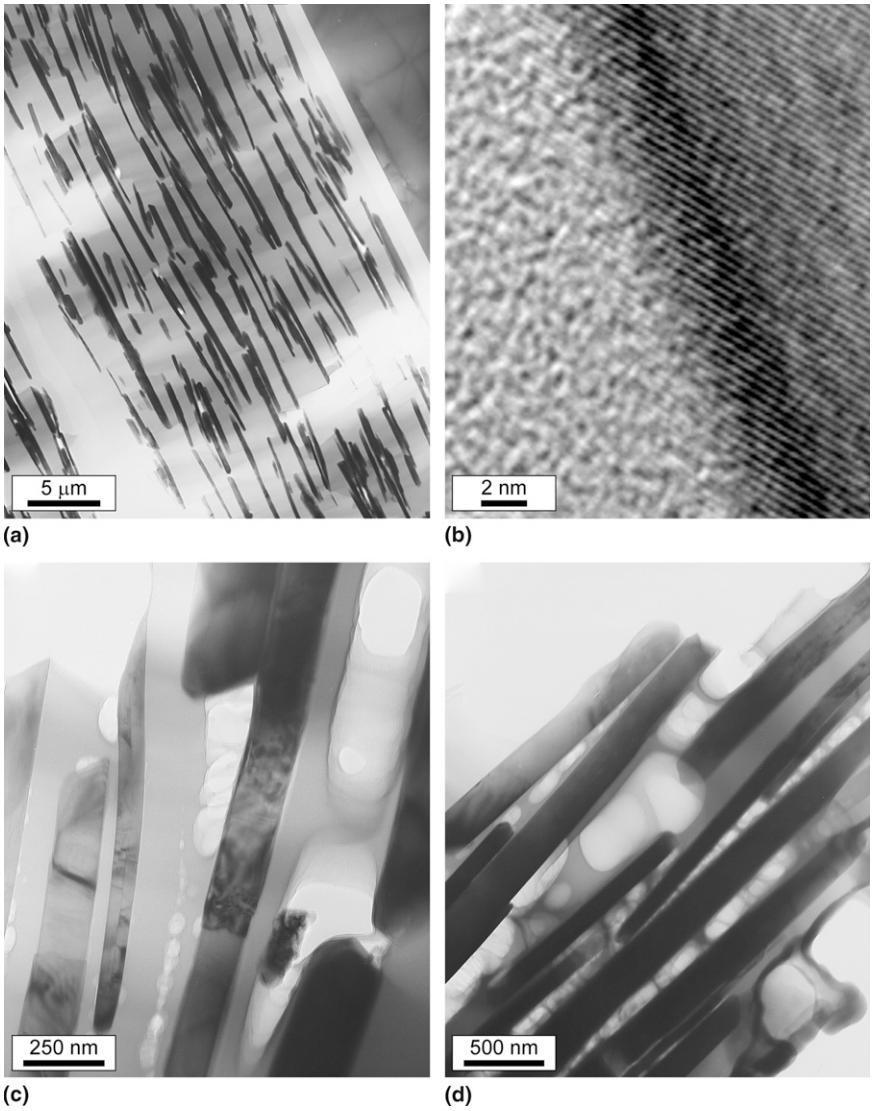

FIG. 3. TEMs of unstrained polyimide matrix composites with volume fractions of APS-modified alumina platelets of (a, b) $V_p \approx 0.18$ and (c, d) $V_p \approx 0.42$, showing an aligned, nearly homogeneously distributed arrangement of alumina platelets parallel to the film surface (a). (c, d) Composites with $V_p > 0.35$ exhibit different types of coalesced pores already before mechanical testing. (b) The high-resolution image indicates that the lattice planes of the alumina platelet (right) terminate undisturbed and immediately at the interface to the polyimide matrix and that the matrix material does not show any structural modification near this interface.

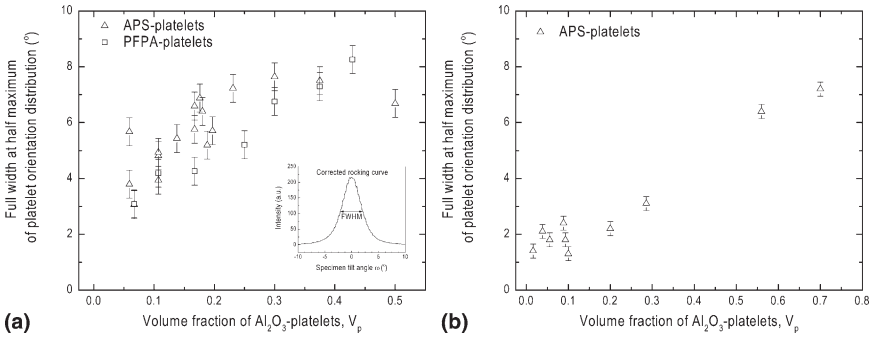

FIG. 4. Degree of platelet orientation indicated by the FWHM of the corrected rocking curves for (a) polyimide and (b) chitosan matrix composites as a function of the platelet volume fraction.

beyond the linear elastic regimen (Fig. 5). When the yield tensile strength of the organic matrix was reached, yielding of the organic matrix between the alumina platelets resulted in significant plastic deformation of the hybrid films. On deformation of the hybrid material, a substantial fraction of the load parallel to the ordered layers is taken by the strong and stiff alumina platelets, increasing the composite's yield strength (σ_y) and elastic modulus (E_c) but gradually decreasing strain at rupture (ε_{rupt}) with increasing V_p.

From these stress-strain curves, σ_y, E_c, and ε_{rupt} of the composites were determined and are shown in Fig. 6 as a function of the platelet volume fraction. Please note that all mechanical plots for polyimide and chitosan have the same axis range for easier comparison.

For composites with a platelet volume fraction lower than ~0.2, both the yield strength and elastic modulus increase, whereas the strain at rupture gradually decreases with increasing V_p. The composites may contain a few voids or pores before deformation, but the platelets do not

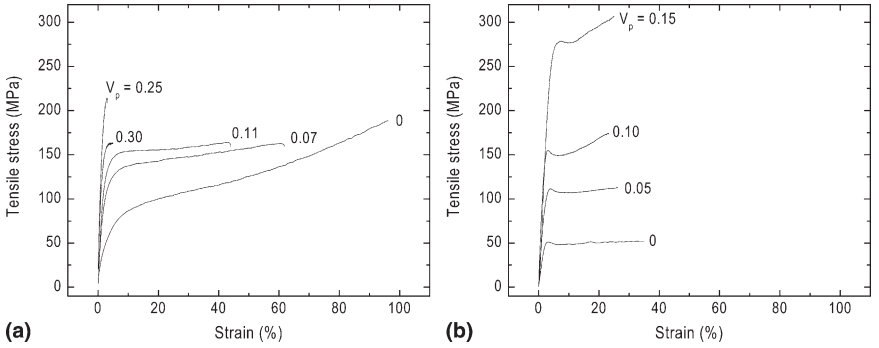

FIG. 5. Tensile stress versus strain curves of (a) polyimide and (b) chitosan matrix composites with increasing platelet concentration. The mechanical properties of the composites are isotropic in the plane of the platelets.

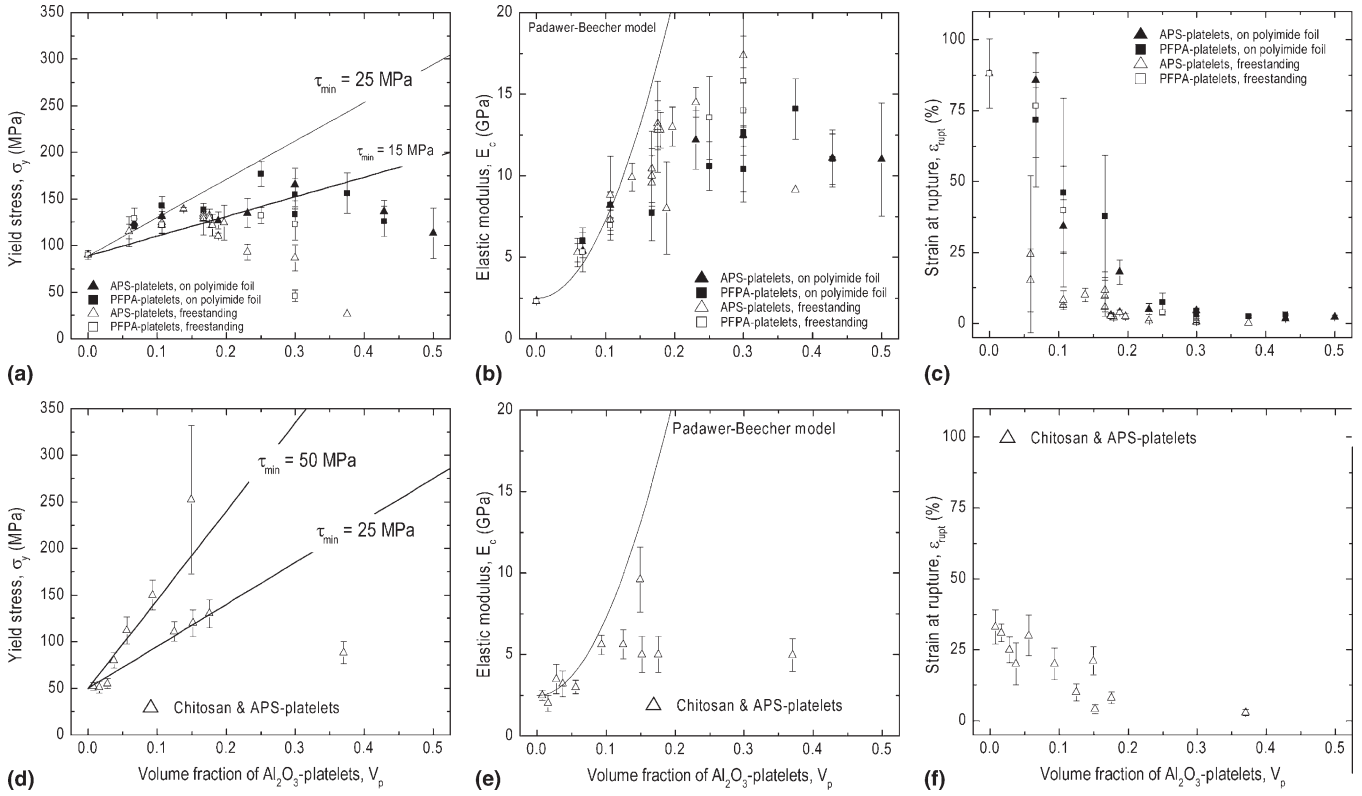

FIG. 6. (a, d) Yield strength, (b, e) elastic modulus, and (c, f) strain at rupture as a function of the platelet volume fraction for (a)–(c) polyimide and (d)–(f) chitosan matrix composites. Predictions of the composites yield strength based on a shear-lag mechanical model[30] are shown in (a) and (d) as full lines assuming different values for the τ_{min} – the lower value of the polymer shear strength or the interfacial-shear strength. Predictions of the elastic modulus based on a model for platelet-reinforced composites[14] are shown as full lines in (b) and (e).

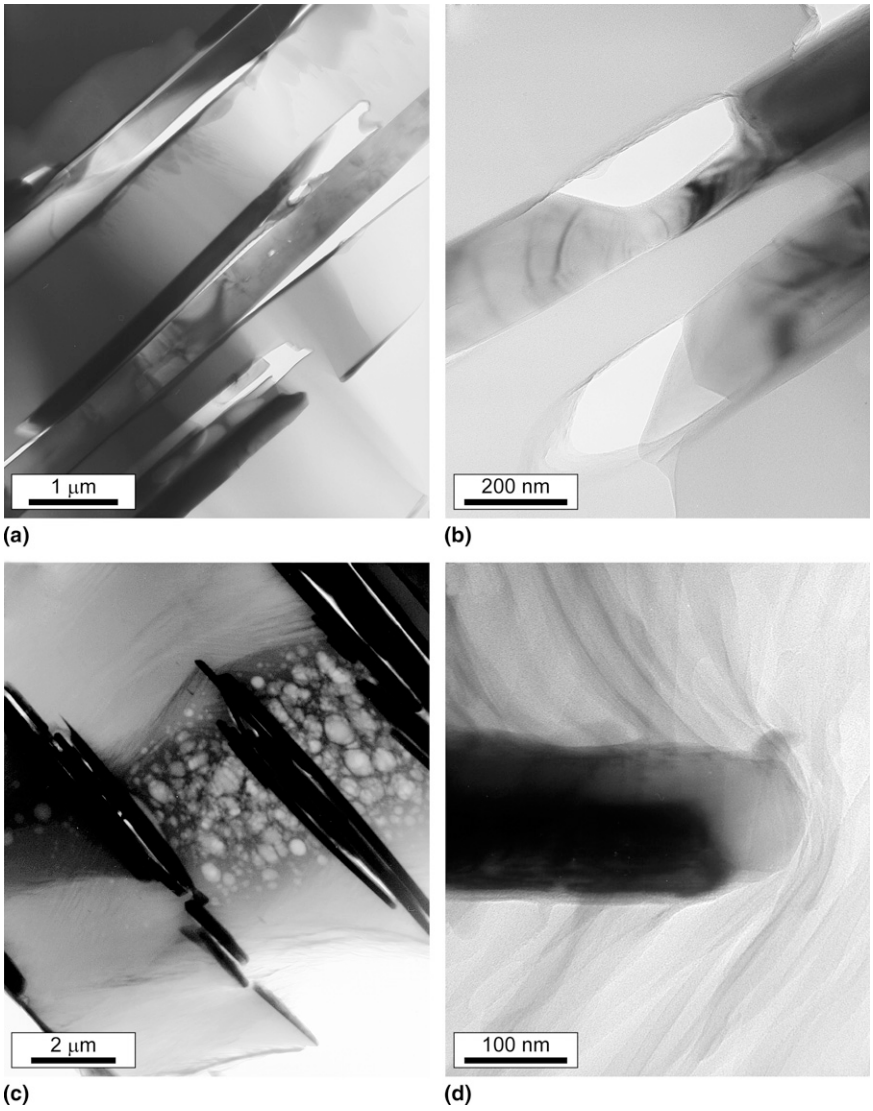

FIG. 7. TEMs of composites with volume fractions of alumina platelets of ≈0.1 after mechanical testing and composite failure. The composites ruptured after (a) 35, (b) 45, and (c, d) 25% tensile strain. The polymer matrix was (a, b) polyimide and (c, d) chitosan. The surface of the platelets was modified with (a, c, d) APS and (b) PFPA.

fracture under the tensile load, allowing for the onset of toughening mechanisms such as friction, debonding, and microcracking at the platelet–polymer interface, as well as plastic deformation and void formation within the polymer matrix. Examples of debonding, platelet pull-out, and flow processes in the polymer matrix are shown by the pore formation at the edge of the platelets in Figs. 7(a) and 7(b) for the polyimide matrix composites after mechanical testing and fracture of the composites. Extensive plastic deformation and void formation within the organic matrix are shown in Figs. 7(c) and 7(d) for the chitosan matrix composites. These observed toughening mechanisms led to very high fracture energies. A rough estimation based on the area under the stress-strain curves indicates that the energy required to fracture our composites is one and two orders of magnitude higher than that needed to rupture natural materials such as nacre[37] or the strongest clay-polymer nanocomposites,[28] respectively. When more and more of the materials volume is filled with stiff ceramic platelets, the organic matrix has to deform more to achieve the same deformation of the composite, thus leading to a strain amplification in the ductile matrix. The strain amplification led to a fully deformed polymer and composite fracture at lower overall strains as the platelet loading increases. Polyimide matrix composites show higher strains until rupture because of the higher intrinsic ability for plastic deformation of polyimide compared with chitosan. The mechanical properties measured on freestanding films and on composite/polymer bilayers are similar in the low-volume fraction range.

Composites with a platelet volume fraction ranging from ∼0.2 to 0.35 broke after the elastic deformation

without substantial plastic flow. The composites deformed 2–4% before fracture. Isolated voids in the unstrained composites, as shown in Fig. 3(a) for a composite with $V_p = 0.18$, are potential sites for stress concentration and crack initiation in the polymeric matrix and might explain the rupture of the composites without significant plastic deformation. Because of the increased platelet content, σ_y and E_c are the highest within this range of volume fractions. Because of the fragility of the hybrid materials, the mechanical properties can only be accurately measured on composite/polymer bilayers where the thin polymer foil prevented damage of the composites before the mechanical tests. Most of the completely freestanding composites with $V_p > 0.2$ broke before their mechanical properties could be measured.

Composites with $V_p > 0.35$ exhibit many large, coalesced pores before mechanical testing, as shown in Figs. 3(c) and 3(d). The polymer layers deposited during spin-coating had to be thin to achieve such high platelet contents. As a result, the inherent small roughness of the underlying platelet layer could not be completely evened out by the thin spin-coated polymer layer. This favors the build up of platelet misalignment (Fig. 4) and the incorporation of voids. Misalignment and the presence of such large pores hindered load transfer from the polymer matrix to the ceramic platelets, decreasing the yield strength and the elastic modulus of the composite. The hybrid films were so fragile that handling of freestanding foils was only possible in the form of composite/polymer bilayers. Typically, such composites fractured quickly at many different locations on the polymer foil, making the determination of the strain at break and calculation of the stress-strain behavior difficult and inexact at these high platelet contents.

At low platelet volume fractions, both the strengthening and stiffening of the composites can be explained by models[14,30] for planar-reinforced bulk composites, as indicated by the predicted curves shown in Fig. 6. The model for the yield strength fits well to the experimental data up to $V_p \approx 0.3$, assuming a τ_{min} within the ranges indicated in Fig. 6. This is valid as long as only the composites measured on the protective polymer foil (full symbols) are considered at $V_p > 0.15$, because these composites are too fragile to be accurately characterized in the form of freestanding films. The elastic modulus predicted by the mechanical model describes the measured properties up to platelet volume fraction of 0.1 accurately. From $V_p = 0.1$ to 0.2, the stiffest composites almost reach the predicted values, but the scattering in the measured values increases. For $V_p > 0.2$, the measured elastic moduli level off at values below the predicted curve because of the processing flaws in the composites at higher platelet volume fractions (Figs. 3 and 4).

The improvements in mechanical properties were caused by load transfer to the platelets as opposed to the strengthening resulting from crystallization or cross-linking effects that are at least partially responsible for the strengthening in nanocomposites.[24,27,28] Crystallization of the polymer was not observed near the polymer–platelet interface in any of our composites. Even on the atomic level, the polymer does not show any structural modification near the organic–inorganic interface as shown by the high-resolution image in Fig. 3(b). The glass transition temperatures (T_g) of the polyimide matrix composites measured by DSC is further evidence that the platelets do not impart any structural changes in the polymeric matrix, because T_g for pure polyimide (325 ± 2 °C) and a composite with $V_p = 0.16$ (328 ± 3 °C) were similar.

Except for the strongest chitosan sample (250 MPa), polyimide and chitosan matrix composites reached similar maximal yield strengths of ~170 MPa. This shows that the reinforcing effect of the platelets was more pronounced in chitosan than in polyimide matrix composites because the yield strength of the pure chitosan (50 MPa) is ~45% lower than that of pure polyimide (90 MPa).

To notably increase the elastic moduli of the composites compared with the matrix alone, a high concentration of platelets is needed. Because of its higher reproducibility during processing, polyimide matrix composites with high platelet volume fractions were more often fabricated than chitosan matrix composites with high V_p. As a result, the highest elastic modulus in reinforced polyimide ($E_c \approx 18$ GPa at $V_p = 0.3$) was almost twice as high as that of the stiffest reinforced chitosan ($E_c \approx 10$ GPa at $V_p = 0.15$).

C. Interfacial bonding

The strength data for $V_p < 0.3$ agrees well with the shown shear-lag mechanical model if τ_{min} is varied from 25 to 50 MPa and from 15 to 25 MPa in chitosan and polyimide matrix composites, respectively. Note that τ_{min} is the lower value of either the interfacial-shear strength (τ_i) or the matrix yield shear strength (τ_y). The τ_{min} values estimated for the chitosan matrix composites were close to or higher than the yield shear strength of the matrix, indicating an efficient interfacial bonding between platelets and polymer in these materials. In contrast, the τ_{min} values estimated for the polyimide matrix composites are lower than the shear yield strength of the polymer, which is an indication of suboptimal bonding at the platelet–polymer interface. If τ_i is lower than τ_y, the strength of the composite is controlled by τ_i rather than τ_y, thus not exploiting the full potential of the material combination.

The lower τ_{min} in polyimide–matrix composites triggered a more detailed study on the surface modification of the platelets. Control experiments made before mechanical testing suggested that APS and PFPA were adsorbed on the surface of the platelets and that even the

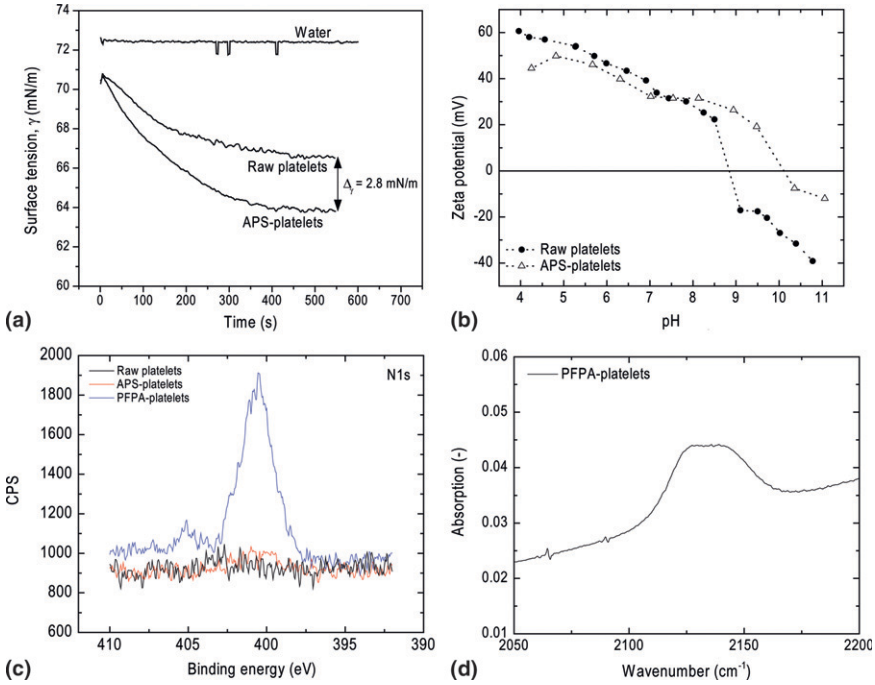

FIG. 8. Contradicting results of the platelet surface modification. Measurement of (a) surface tension and (b) isoelectric point indicated that the APS is attached to the platelet surface, whereas more accurate (c) XPS investigation showed no sign of nitrogen and therefore APS on the platelets. The presence of PFPA and its intact functional azide group was confirmed by (c) XPS and (d) FTIR. Because the PFPA needs to bind to the (missing) APS to be covalently linked to the alumina, it is likely that the PFPA was only physically adsorbed to the platelets.

functional azide group in the PFPA was still intact. Figure 8(a) shows that the APS-coated platelets adsorb to a larger extent to an air–water interface compared with the bare platelets, as indicated by the stronger drop in surface tension achieved in the presence of the surface modifier. This is presumably caused by the higher hydrophobicity of platelets coated with APS. The shift in the isoelectric point of platelets treated with APS is a further indication that the surface modifier indeed adsorbed on the platelet surface [Fig. 8(b)]. More detailed XPS analysis showed later that only PFPA but not APS was present on the oxide surface [Fig. 8(c)]. The presence of intact azide groups in the PFPA molecules adsorbed on the platelet surface was confirmed by FTIR [Fig. 8(d)]. Residual unreacted APS in the solvent and changes in the platelet size distribution caused by repeated centrifugation during the surface modification procedure could be responsible for the inaccurate outcome of the initial control experiments. Because PFPA has to bind to APS to be covalently linked to the alumina surface, it is likely that the PFPA molecules were only physically adsorbed to the platelets. The presence of fluorine on the surface of the bare platelets, which is a residue from the synthesis,[38] presumably disturbed the surface modification with APS. These results suggest that the polymer in the matrix interacts with the platelets through van der Waals forces and hydrogen bonding rather than through covalent bonds with APS or PFPA. The absence of APS on the platelet surface was not detrimental to the τ_{min} in the case of the chitosan composites. This might be explained by the fact that chitosan has a high density of polar and chargeable function groups such as $–NH_2$ and –OH that can bind to the polar groups on the surface of the alumina platelets (e.g., –OH) through hydrogen bonding and van der Walls interactions. Electrostatic interactions between the chitosan polymer and the platelet surface are not expected to play a major role because of the high concentration of acetic acid counter-ions (0.34 mol/L) present in the aqueous chitosan solution used for spin-coating. It is also important to note that, in these composites, the APS surface modification was only supposed to increase the hydrophobicity of the alumina platelets to enable their adsorption to the air–water interface during the composite assembly rather than to covalently link the platelets to the chitosan. However, in the case of polyimide composites, the APS was intended to covalently bond the polymer to the platelets. The absence of APS on the platelet surface made this covalent bonding impossible and thus led to rupture of the interface before yielding of the polymer. This explains the lower interfacial strength values obtained by fitting the yield stress data of the polyimide-based composites with the shear-lag mechanical model.

As opposed to the interface-controlled fracture of the polyimide-based materials ($\tau_i < \tau_y$), the stronger platelet–polymer interface in the chitosan–matrix composites ($\tau_i > \tau_y$) led to a more pronounced reinforcing

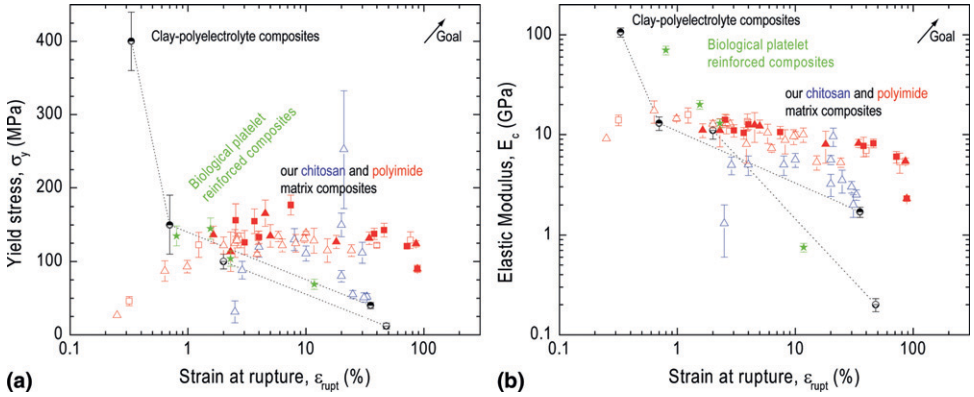

FIG. 9. Yield strength and elastic modulus as a function of the strain at rupture for different platelet-reinforced composites and their matrices. The platelet volume fraction increases from right to left. Our composites are compared with biological platelet-reinforced structures and the strongest in-plane textured clay-polyelectrolyte composites from Refs. 28 and 31.* The mechanical properties from nacre (red abalone, *Haliotis rufescens*), bone, dentin, and calcified tendon were obtained from Wang et al.,[37] Landis et al. (after Ashman),[39] Sano et al.,[40] and Landis et al.,[39] respectively. *$\sum rupt$ for composites from Ref. 31 was estimated to 2%, instead of the reported 10%, because these samples only carry considerable load for strain values >8%.

effect because fracture in this case initiates within the ductile polymeric phase rather than at the interface. Although fracture occurred through the pull-out mode in both composites, the difference in interfacial strength strongly influenced the composite yield stress and the toughening mechanisms involved. Cross-sections of fractured composites show that platelets in the polyimide-based materials are pulled out of the surrounding matrix, as indicated by the pores formed at the ends of the inorganic platelets shown in Figs. 7(a) and 7(b). In the chitosan matrix composites, on the other hand, fracture at the platelet–polymer interface is not observed. Instead, pores form in the organic matrix in between the layers of platelets as a result of the strong plastic deformation of the polymer [Figs. 7(c) and 7(d)]. The two different fracture mechanisms for the different matrix polymers prove that the polyimide–platelet interface yielded before the polyimide matrix, whereas the chitosan–alumina interface is stronger than the polymer itself, causing void formation within the matrix. These results indicate the importance of controlling the strength of the platelet–polymer interface for the preparation of composites with predictable and tunable mechanical behavior.

D. Comparison with other platelet-reinforced composites

The combination of high yield strength and high strain at rupture caused by plastic deformation of the polymeric matrix is the most distinctive feature of our hybrid materials compared with other platelet-reinforced composites as shown in Fig. 9. Polymer films containing up to ~20 vol% of alumina platelets showed inelastic deformation (ε_{inel}) in the range 2–90%, as opposed to the brittle failure observed in the strongest clay-reinforced polymers ($\varepsilon_{inel} = 0$).[28]

The strength and ductility of our platelet-reinforced polymers were also higher than the values obtained for natural hybrid materials such as nacre and bone. The higher strength at lower platelet concentrations resulted from the enhanced tensile strength of the synthetic alumina platelets used in the artificial composites compared with the aragonite platelets found in nacre.[29] Higher platelet strength allowed for the use of artificial platelets with a higher aspect ratio while keeping the composite fracture under the platelet pull-out mode.

The elastic modulus of the fabricated composites reached values almost as high as that of human bone ($E \approx 20$ GPa) but still lower than the values of 70 and 100 GPa reported for nacre[37] and for the stiffest clay/polymer nanocomposites,[28] respectively. The lower elastic moduli of our composites result from the lower content of platelets ($V_p < 0.35$) compared with nacre ($V_p = 0.95$) and the stiffest clay–polymer nanocomposites ($V_p = 0.5$).

V. CONCLUSIONS

We fabricated highly oriented planar-reinforced composites consisting of submicrometer-thin alumina platelets embedded in either a chitosan or a polyimide organic matrix. By choosing platelets with an aspect ratio slightly below a critical value, the strength and stiffness of the composite were maximized while keeping the fracture under platelet pull-out mode. This led to hybrid artificial materials that are simultaneously strong, stiff, and ductile. The strengthening and stiffening effects achieved with these composites result from an effective load transfer from the organic matrix to the inorganic platelets and were successfully described by a simple shear-lag mechanical model. The high ductility was accompanied by the onset of several toughening mechanisms such as frictional sliding, debonding, and microcracking at the

platelet–polymer interface, as well as void formation and plastic deformation within the matrix. Up to a platelet volume fraction of ~0.2, the reinforced polymers exhibit high strength, stiffness, and ductility. For platelet volume fractions between 0.2 and 0.35, a moderate increase in strength and stiffness is still observed at the expense of plastic deformation. However, all properties strongly degrade for platelet volume fractions >0.35 because of platelet misalignment and the incorporation of voids during processing. The strength of the platelet–polymer interface strongly influenced the yield strength and the toughening mechanisms of the composites. The weaker interfacial bonding obtained for the polyimide-matrix materials led to a moderate reinforcing efficiency and to frictional sliding and debonding as main sources of toughening. In contrast, the chitosan-based composites exhibited stronger interfacial strength, resulting in higher reinforcing efficiency and extensive plastic deformation and void formation in the matrix. Despite the lower relative strength improvement achieved, the polyimide films were of similar absolute strength, generally more ductile, chemically more inert (e.g., humidity insensitivity), and more reproducible during processing than the chitosan matrix films. In comparison with clay–polymer artificial composites and natural platelet-reinforced materials, our composites are more ductile at similar strength or stiffness but do not reach the same ultimate strength and stiffness of the strongest clay-reinforced polymers or the stiffness of nacre because of the lower content of platelets. The development of new approaches to avoid the incorporation of defects in composites with high platelet concentrations and to deliberately control bonding at the platelet–polymer interface should allow for the fabrication of hybrid materials with tunable and further improved mechanical properties.

ACKNOWLEDGMENTS

Financial support from ETH Zürich and Ciba is thankfully acknowledged. We also thank Prof. M. Yan (Portland State University) for kindly providing the functionalized perfluorophenyl-azide used for surface modification; V. Klass, I. Olliges, C. Müller, T. Goren, and S. Pemberton for their contribution to the experimental part of this work; and the polymer technology group and the laboratory for surface science and technology at ETH Zürich for sharing their equipment and many fruitful discussions.

REFERENCES

1. H.A. Lowenstam and S. Weiner: *On Biomineralization* (Oxford University Press, New York, 1989), pp. IX, 324.
2. M. Sarikaya, J. Liu, and I.A. Aksay: Nacre: Properties, crystallography, morphology, and formation, in *Biomimetics Design and Processing of Materials*, edited by M. Sarikaya and I.A. Aksay (AIP Press, Woodbury, NY, 1995), pp. XI, 285.
3. G. Mayer: Rigid biological systems as models for synthetic composites. *Science* **310,** 1144 (2005).
4. A. Lin and M.A. Meyers: Growth and structure in abalone shell. *Mater. Sci. Eng., A* **390,** 27 (2005).
5. M. Rousseau, E. Lopez, P. Stempfle, M. Brendle, L. Franke, A. Guette, R. Naslain, and X. Bourrat: Multiscale structure of sheet nacre. *Biomaterials* **26,** 6254 (2005).
6. N. Nassif, N. Pinna, N. Gehrke, M. Antonietti, C. Jager, and H. Colfen: Amorphous layer around aragonite platelets in nacre. *Proc. Nat. Acad. Sci. U.S.A.* **102,** 12653 (2005).
7. J.D. Currey: Mechanical-properties of mother of pearl in Tension. *Proc. R. Soc. London, Ser. B* **196,** 443 (1977).
8. A.P. Jackson, J.F.V. Vincent, and R.M. Turner: The mechanical design of nacre. *Proc. R. Soc. London, Ser. B* **234,** 415 (1988).
9. H.D. Wagner and S. Weiner: On the relationship between the microstructure of bone and its mechanical stiffness. *J. Biomech.* **25,** 1311 (1992).
10. I. Jager and P. Fratzl: Mineralized collagen fibrils: A mechanical model with a staggered arrangement of mineral particles. *Biophys. J.* **79,** 1737 (2000).
11. A.G. Evans, Z. Suo, R.Z. Wang, I.A. Aksay, M.Y. He, and J.W. Hutchinson: Model for the robust mechanical behavior of nacre. *J. Mater. Res.* **16,** 2475 (2001).
12. H.J. Gao, B.H. Ji, I.L. Jager, E. Arzt, and P. Fratzl: Materials become insensitive to flaws at nanoscale: Lessons from nature. *Proc. Nat. Acad. Sci. U.S.A.* **100,** 5597 (2003).
13. F. Barthelat, H. Tang, P.D. Zavattieri, C.M. Li, and H.D. Espinosa: On the mechanics of mother-of-pearl: A key feature in the material hierarchical structure. *J. Mech. Phys. Solids* **55,** 306 (2007).
14. G.E. Padawer and N. Beecher: On strength and stiffness of planar reinforced plastic resins. *Polym. Eng. Sci.* **10,** 185 (1970).
15. J. Lusis, R.T. Woodhams, and M. Xanthos: Effect of flake aspect ratio on flexural properties of mica reinforced plastics. *Polym. Eng. Sci.* **13,** 139 (1973).
16. J. Rexer and E. Anderson: Composites with planar reinforcements (flakes, ribbons)—Review. *Polym. Eng. Sci.* **19,** 1 (1979).
17. N. Almqvist, N.H. Thomson, B.L. Smith, G.D. Stucky, D.E. Morse, and P.K. Hansma: Methods for fabricating and characterizing a new generation of biomimetic materials. *Mater. Sci. Eng., C* **7,** 37 (1999).
18. S.S. Ray and M. Okamoto: Polymer/layered silicate nanocomposites: A review from preparation to processing. *Prog. Polym. Sci.* **28,** 1539 (2003).
19. S. Deville, E. Saiz, R.K. Nalla, and A.P. Tomsia: Freezing as a path to build complex composites. *Science* **311,** 515 (2006).
20. E. Munch, M.E. Launey, D.H. Alsem, E. Saiz, A.P. Tomsia, and R.O. Ritchie: Tough, bio-inspired hybrid materials. *Science* **322,** 1516 (2008).
21. E.R. Kleinfeld and G.S. Ferguson: Stepwise formation of multilayered nanostructural films from macromolecular precursors. *Science* **265,** 370 (1994).
22. S. Stankovich, D.A. Dikin, G.H.B. Dommett, K.M. Kohlhaas, E.J. Zimney, E.A. Stach, R.D. Piner, S.T. Nguyen, and R.S. Ruoff: Graphene-based composite materials. *Nature* **442,** 282 (2006).
23. P.B. Messersmith and E.P. Giannelis: Synthesis and characterization of layered silicate-epoxy nanocomposites. *Chem. Mater.* **6,** 1719 (1994).
24. D. Schmidt, D. Shah, and E.P. Giannelis: New advances in polymer/layered silicate nanocomposites. *Curr. Opin. Solid State Mater. Sci.* **6,** 205 (2002).
25. N. Sheng, M.C. Boyce, D.M. Parks, G.C. Rutledge, J.I. Abes, and R.E. Cohen: Multiscale micromechanical modeling of polymer/clay nanocomposites and the effective clay particle. *Polymer* **45**(2), 487 (2004).

26. D. Hull and T.W. Clyne: *An Introduction to Composite Materials*, 2nd ed. (Cambridge University Press, Cambridge, 1996), p. 326.
27. A. Okada and A. Usuki: The chemistry of polymer-clay hybrids. *Mater. Sci. Eng., C* **3,** 109 (1995).
28. P. Podsiadlo, A.K. Kaushik, E.M. Arruda, A.M. Waas, B.S. Shim, J.D. Xu, H. Nandivada, B.G. Pumplin, J. Lahann, A. Ramamoorthy, and N.A. Kotov: Ultrastrong and stiff layered polymer nanocomposites. *Science* **318,** 80 (2007).
29. L.J. Bonderer, A.R. Studart, and L.J. Gauckler: Bioinspired design and assembly of platelet reinforced polymer films. *Science* **319,** 1069 (2008).
30. B. Glavinchevski and M. Piggott: Steel disk reinforced polycarbonate. *J. Mater. Sci.* **8,** 1373 (1973).
31. Z.Y. Tang, N.A. Kotov, S. Magonov, and B. Ozturk: Nanostructured artificial nacre. *Nat. Mater.* **2,** 413 (2003).
32. S. Krohn: Characterization and applications of short-chain chitosans. Ph.D. dissertation, Christian-Albrechts-Universität, Kiel, Germany, 2003.
33. M.A. Bartlett and M.D. Yan: Fabrication of polymer thin films and arrays with spatial and topographical controls. *Adv. Mater.* **13,** 1449 (2001).
34. F. Macionczyk: Determination of mechanical properties of thin Al and AlCu-layers on polyimide foils by tensile testing. Ph.D. dissertation, Shaker, Aachen, Germany, 1999, p. 131.
35. M.D. Vaudin, M.W. Rupich, M. Jowett, G.N. Riley, and J.F. Bingert: A method for crystallographic texture investigations using standard x-ray equipment. *J. Mater. Res.* **13,** 2910 (1998).
36. M.D. Vaudin: *Software TexturePlus* (NIST, Gaithersburg, MD, 2006).
37. R.Z. Wang, Z. Suo, A.G. Evans, N. Yao, and I.A. Aksay: Deformation mechanisms in nacre. *J. Mater. Res.* **16,** 2485 (2001).
38. J.S. Robinson, L.M. Cukrov, T. Tsuzuki, D.A. Lee, P.G. McCormick, J. Robinson, L. Heatley, D. Lee, P. McCormick, and L.M. Heatley: Process for the production of ultrafine plate-like alumina particles. Patent No. WO/2004/060804 (July 22, 2004).
39. W.J. Landis, J.J. Librizzi, M.G. Dunn, and F.H. Silver: A study of the relationship between mineral-content and mechanical-properties of turkey gastrocnemius tendon. *J. Bone Miner. Res.* **10,** 859 (1995).
40. H. Sano, B. Ciucchi, W.G. Matthews, and D.H. Pashley: Tensile properties of mineralized and demineralized human and bovine dentin. *J. Dent. Res.* **73,** 1205 (1994).